Cement & Concrete Composites 31 (2009) 721–730

Contents lists available at ScienceDirect

Cement & Concrete Composites

journal homepage: www.elsevier.com/locate/cemconcomp

Cracking mechanisms in durable sisal fiber reinforced cement composites

Flávio de Andrade Silva [a], Barzin Mobasher [b,*], Romildo Dias Toledo Filho [a]

[a] Department of Civil Engineering, COPPE/ Universidade Federal do Rio de Janeiro, P.O. Box 68506, CEP 21941-972, Rio de Janeiro – RJ, Brazil
[b] Department of Civil and Environmental Engineering, Arizona State University, P.O. Box 875306, Tempe, AZ 5287-5306, USA

ARTICLE INFO

Article history:
Received 21 February 2008
Received in revised form 13 March 2009
Accepted 24 July 2009
Available online 30 July 2009

Keywords:
Natural fiber
Cement composites
Crack formation
Image analysis

ABSTRACT

Fiber reinforced cement composite laminates with long sisal fibers were manufactured using a cast hand lay up technique. A matrix with partial cement replacement by metakaolin and calcined waste crushed clay brick was used in order to improve the durability aspects. Mechanical response was measured under tension and bending tests while crack formation was investigated using a high resolution image capturing procedure. Crack spacing was measured using image analysis and correlated with the applied strain under both the tensile and bending response. Various stages of loading corresponding to initiation, propagation, distribution, opening, and localization of a crack system in the specimen are discussed. The effect of flexural cracking on the location of neutral axis during the bending tests was measured using strain-gages.

1. Introduction

The need for economical, sustainable, safe, and secure shelter is an inherent global problem and numerous challenges remain in order to produce environmentally friendly construction products which are structurally safe and durable. This paper addresses the development of strain hardening cement composites using sisal, a natural fiber with an average tensile strength of 400 MPa and strain at failure of 3% as reinforcement in concrete. These composites provide an exciting opportunity to the housing construction industry and may generate economic incentives particularly in developing countries since the availability and production of composite reinforcement requires a low degree of industrialization. Furthermore, in comparison to the most common synthetic reinforcing fibers, natural fibers require less energy to produce and are the ultimate green products.

Natural fibers have been traditionally used as a substitute of asbestos in the form of chopped, short, and/or in a pulp form for the production of thin elements for roofing and cladding. An increased use of these materials for applications such as cladding, internal, and external partitioning walls is possible and may lead towards the development of low cost-sustainable materials [1–8]. Natural fiber cement composites have been mainly reinforced by short or pulp cellulose fibers. Nevertheless, their application in the construction industry is still quite limited due to the lack of understanding in how to improve the durability while making ductile materials.

Continuous fiber reinforced cement based composites are a new class of sustainable construction materials with superior tensile strength and ductility [9,10]. The enhanced strength and ductility is primarily governed by the composite action that exists such that the fibers bridge the matrix cracks and transfer the loads, allowing a distributed microcrack system to develop. These materials are strong enough to be used as load bearing structural members, in applications such as structural panels, impact and blast resistance, repair and retrofit, earthquake remediation, strengthening of unreinforced masonry walls, and beam-column connections [11].

Vegetable fiber cement composites produced with ordinary Portland cement matrices undergo an aging process in humid environments during which they may suffer a reduction in post-cracking strength and toughness. The aging process is due to fiber mineralization and results in reducing the tensile strength of fibers and decreasing the fiber pullout ligament after fracture. This mineralization process is a result of migration of hydration products (mainly $Ca(OH)_2$) to the fiber structure. Efforts to develop durable and structural cement composite laminates reinforced with long sisal fibers has shown much promise recently [12,13]. A recently developed matrix that lowers Calcium Hydroxide production (only 50% Portland cement as compared to conventional systems) increases the long term durability of natural fiber, reduces CO_2 emissions, and presents an economical and sustainable approach. The modified matrix has shown no strength and toughness reduction in accelerated aging tests [13]. The present study is focused on the implementation of this matrix in lieu of a Portland cement matrix which invariably results in a low durability performance record [13].

A fundamental understanding in toughening mechanisms and how cracks form and propagate in the brittle matrix composites

* Corresponding author. Tel.: +1 480 965 0141; fax: +1 480 965 0557.
E-mail address: barzin@asu.edu (B. Mobasher).

0958-9465/$ - see front matter © 2009 Elsevier Ltd. All rights reserved.
doi:10.1016/j.cemconcomp.2009.07.004

is important for optimization, analysis, and design. The cracking mechanism in a multilayer sisal fiber reinforced composite is addressed in this paper. An experimental procedure was used to monitor and analyze the distributed cracking formation, the stiffness degradation, and the crack spacing distribution functions during flexural bending and tensile tests. Photographs of the crack formation at periodic strain levels were processed by image-analysis techniques and correlated with the applied stress levels. The differences between the flexural results and tensile results were studied by comparing the strain distribution profiles in the loading configuration. In the tension test, the strain distribution was verified by the uniform nature of cracking across the specimen, whereas in the flexural test, the movement of the neutral axis was experimentally determined by strain-gages attached to compression and tensile composite surfaces. Analysis of the flexural strains allows a direct comparison between material properties obtained from tensile and flexural data.

2. Experimental program

2.1. The sisal fiber

The sisal fibers used in this investigation were extracted from the sisal plant in a farm located in the city of Valente, state of Bahia – Brazil. The sisal plant leaf is a functionally graded composite structure which is reinforced by three types of fibers: structural, arch, and xylem fibers. The first occurs in the periphery of the leaf providing resistance to tensile loads (see Fig. 1). The others present secondary reinforcement, occurring in the middle of the leaf, as well as, a path for nutrients. The fibers were characterized earlier to have an irregular cross-section with mean area ranging from 0.04 to 0.05 mm^2 and a mean density, elastic modulus, and tensile strength of 0.9 g/cm^3, 19 GPa and 400 MPa, respectively [14].

Sisal fibers contain numerous elongated fiber-cells which are about 6 to 30 μm in diameter [15]. The microstructure of the

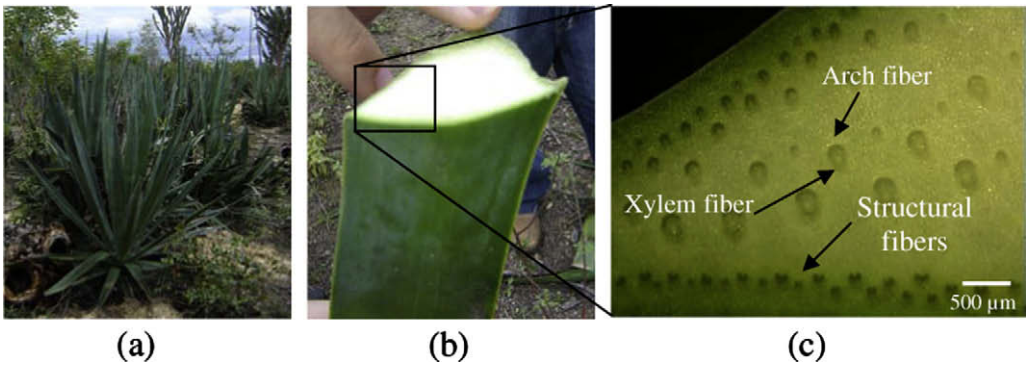

Fig. 1. The sisal plant (a), leaf (b) and leaf cross-section showing different fiber types (c) [14].

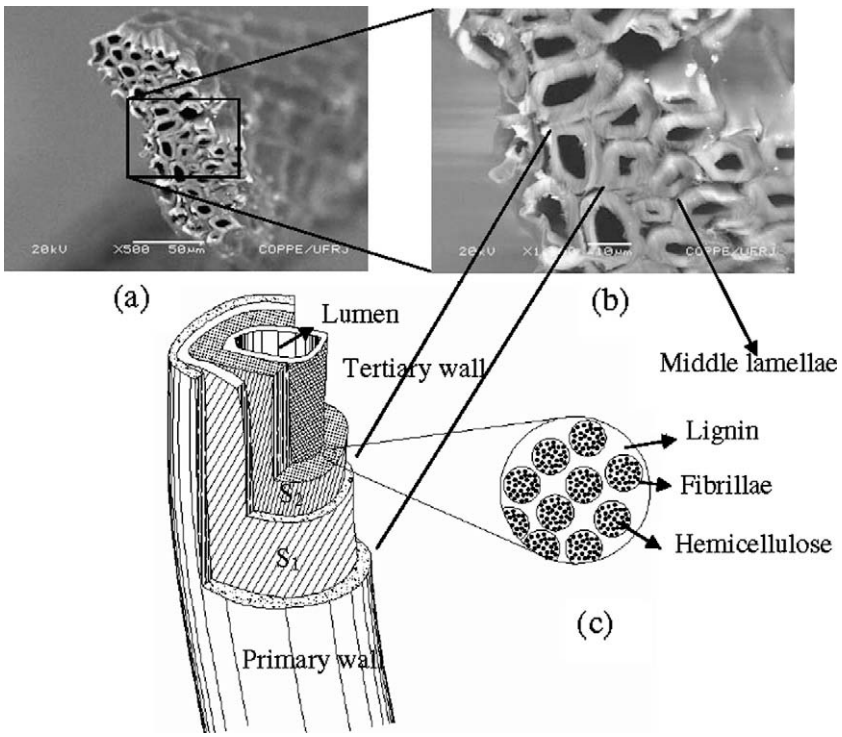

Fig. 2. Fiber-cell microstructure: (a) cross-section view showing the fiber-cells, lumens and middle lamellae, (b) magnification of the cross-section and (c) schematic drawing showing the different layers of an individual fiber-cell [13].

fiber-cell is shown in Fig. 2. The individual fiber-cells are linked together by means of the middle lamella, which consist of hemicellulose and lignin. The lumen varies in size but its shape is usually well-defined (see Fig. 2b). Each individual fiber-cell is made up of four main parts, namely the primary wall, the thick secondary wall, the tertiary wall and the lumen (see Fig. 2c).

After receiving the sisal fibers they were washed and cut to the size of the molds (400 mm). The fibers were weighted and separated into five different layers resulting in a total volume fraction of 10% (see Section 2.3). The sisal fibers were stitched by three cotton fibers to make a homogeneous spacing between the fibers so as to facilitate the molding process.

2.2. Matrix modification

To increase the durability of the composites, the cementitious matrix consisted on 50% Portland cement, 30% metakaolin (MK), and 20% calcined waste crushed clay brick (CWCCB) [12,13]. Portland cement CPII F-32 defined by the Brazilian standard [16] as composed with filler (in mass: 85% < clinker < 91%; 3% <

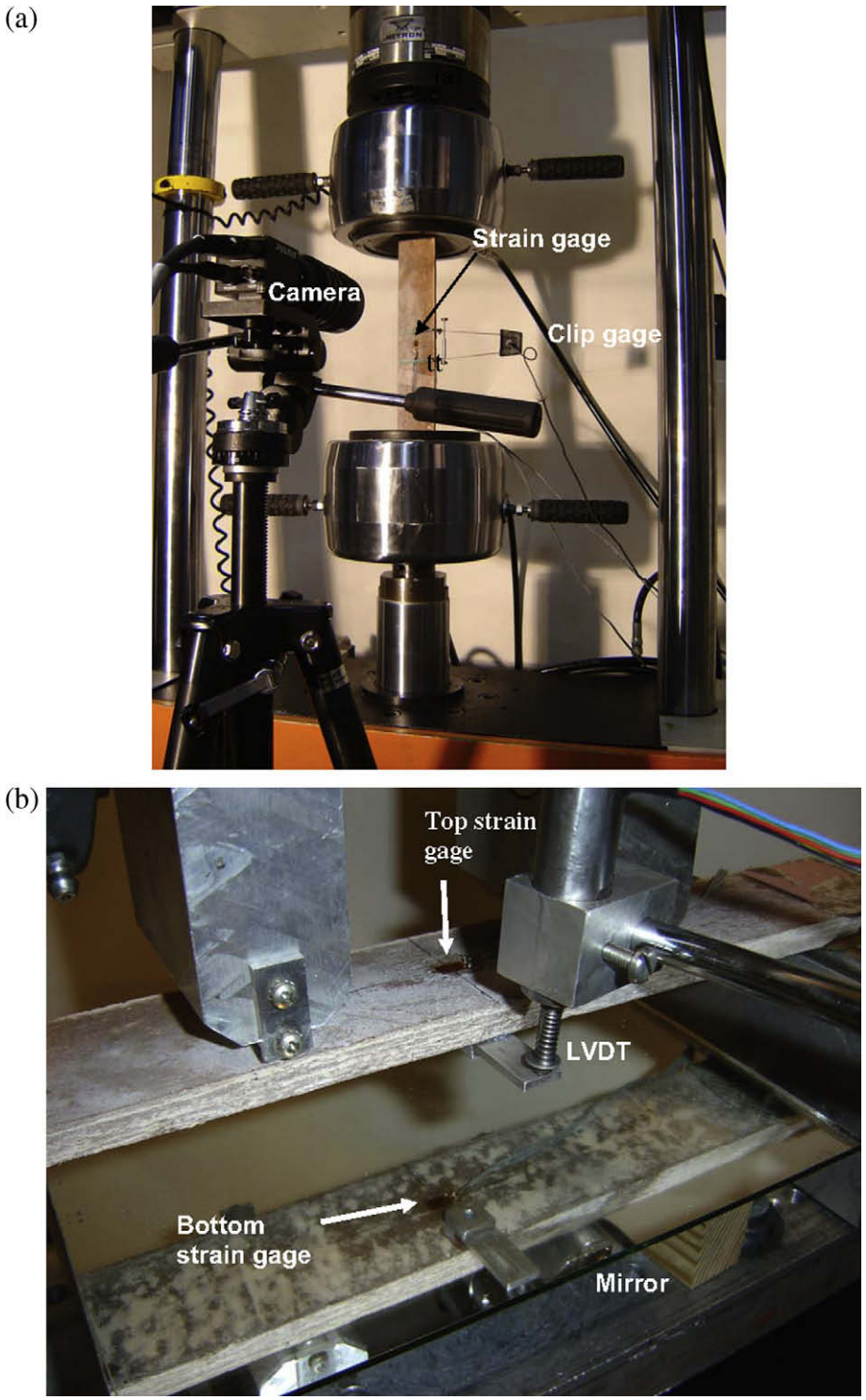

Fig. 3. Mechanical tests set-up: (a) direct tension and (b) four-point bending.

gypsum < 5%; 6% < filler < 10%) with a 28 days compressive strength of 32 MPa was used. The metakaolin (MK) was obtained from Metacaulim do Brasil Industria e Comércio LTDA, and calcined waste crushed clay brick (CWCCB) from an industry located in Itaborai – RJ, Brazil, calcined at 850 °C. The mortar matrix used a mix proportion of 1:1:0.4 (cementitious material:sand:water by weight). River sand with a maximum diameter of 1.18 mm and density of 2.67 g/cm^3 and a naphthalene superplasticizer Fosroc Reax Conplast SP 430 with content of solids of 44% were used.

Wollastonite is a naturally occurring white, non-metallic mineral with an acicular morphology. Wollastonite fiber (JG class, $CaSiO_3$), obtained from Energyarc, with an average equivalent diameter of 40 μm and an aspect ratio of 15 was used as a micro-reinforcement in the composite production (V_f = 5%).

2.3. Composite manufacturing

The matrix was produced using a bench-mounted mechanical mixer of 20 L capacity. The cementitious materials were homogenized by dry mixing for 30 s prior to addition of sand and 5% by volume of wollastonite. The powder material was mixed for and additional 30 s prior to addition of superplasticizer and water. The mixture was blended for 3 min. Laminates were produced by placing the mortar mix in a steel mold, one layer at a time, followed by single layers of long unidirectional aligned fibers (up to 5 layers). The samples were consolidated using a vibrating table operated at a frequency of 65 Hz, and resulted in a sisal fiber volume fraction of 10%. After casting, composites were compressed at 3 MPa for 5 min. The compression load was applied in the face that the matrix was placed. The specimens were covered in their molds for 24 h prior to moist curing for 28 days in a cure chamber with 100% RH and 23 ± 1 °C.

3. Testing

3.1. Mechanical performance

Direct tensile tests were performed in a closed loop servohydraulic testing machine with a capacity of 500 kN (see Fig. 3a). The tests were controlled by the cross-head displacement at a rate of 0.1 mm/min. Six specimens measuring 400 mm × 50 mm × 12 mm (length × width × thickness) were tested using a gage length of 300 mm with fixed–fixed boundary conditions. Aluminum thin sheets were glued on both ends of the specimen and the pressure of the hydraulic grips was adjusted to 1.37 MPa (200 psi) in order to minimize stress concentration and damage. The tensile load, cross-head displacement and strain were recorded. Tensile strains were also measured by a strain gage glued on the center of the specimen.

Four-point bending tests were performed in a MTS 810 universal testing machine with a capacity of 100 kN. The tests were controlled by the cross-head displacement at a rate of 0.5 mm/min. Six specimens measuring 400 mm × 70 mm × 12 mm (length × width × thickness) were tested under a span of 300 mm. Strain-gages were glued at the center bottom and top surface of the specimen in order to compute the extreme fiber strain and the neutral axis (see Fig. 3b). The bending load, cross-head displacement and strains were recorded.

3.2. Crack spacing measurements

By evaluating cracking patterns at regular time intervals, crack development throughout the loading cycle of tensile and bending test were recorded. A digital Pulnix camera with a 10× macro zoom lens and frame grabber captured images of 480 × 640 in resolution at 60 s intervals. Images were used to measure the crack formation during bending and tension tests. Photos of the tension face in bending tests were taken using a mirror positioned at 45° with respect to the specimen as shown in Fig. 3b.

Image processing was done by the digital processing toolbox of MATLAB. To quantitatively measure the crack spacing as a function of the applied strain, a two step approach was used. During the first step, newly formed cracks of each image were traced and added to data from previous loading increment. Fig. 4a represents the crack development at a strain of 0.0068 mm/mm. The trace profiles of these cracks are shown in Fig. 4b. The second step measured the crack spacing from the traced cracks as shown in Fig. 4c using the following procedure.

An image consisting of a series of parallel lines was generated. The crack spacing was measured in pixels, and the image was calibrated using conventional techniques to convert the size of a pixel to length measures. By conducting a binary "AND" operation the points of intersection of the series of parallel lines with the cracks were identified. A second binary operation of "OR" between the intersection points and the parallel spacing lines, broke up the straight lines into segments representing crack spacing distribution as shown in Fig. 4c. The distribution of the length segments and statistical parameters of crack spacing were computed next [17–19].

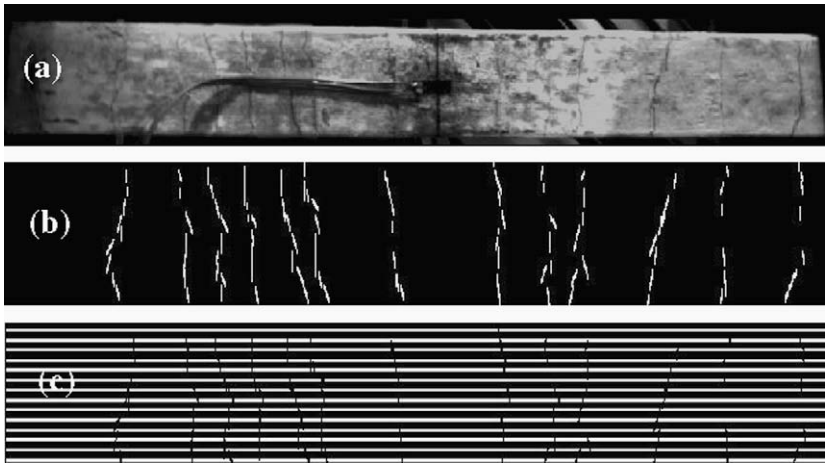

Fig. 4. Image-analysis methodology: (a) image during tensile test, (b) trace lines of cracking and (c) horizontal line segments representing the distribution of crack spacing.

4. Results and discussion

4.1. Mechanical tests

Fig. 5 shows a typical tensile stress strain response of the sisal fiber reinforced composite system. Two measures of tensile strain are used including the localized strain measured from the electrical resistance gage and the nominal strain defined by dividing the cross-head stroke displacement by the specimen length. Comparison of the two strain measurements allows one to evaluate the early age cracking phase and make a distinction among all stages of cracking. These responses differ at various stages of loading as they correspond to crack initiation, propagation, distribution, opening, and localization.

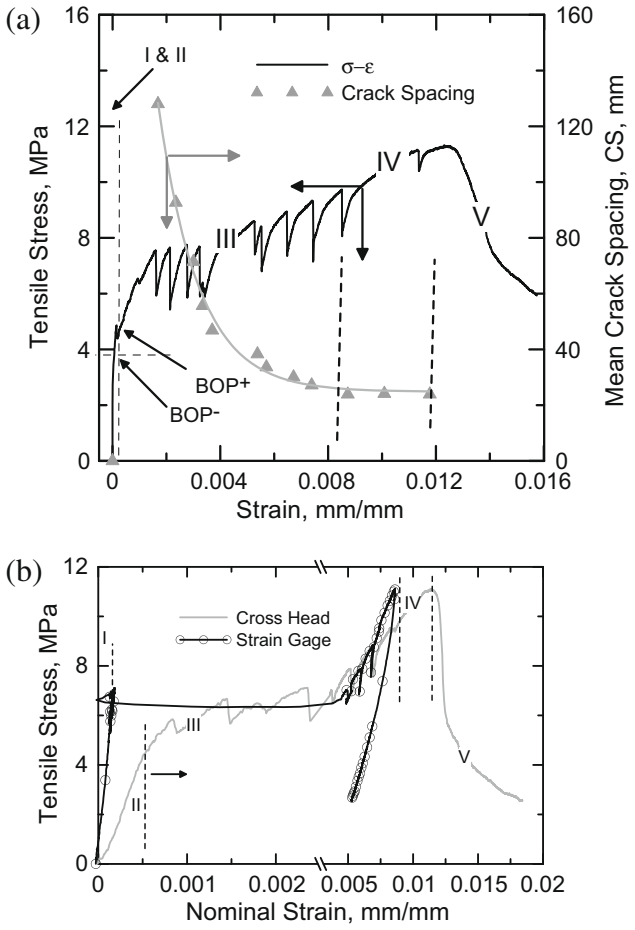

Fig. 5. Tensile response of the sisal fiber reinforced composite system: (a) tensile stress and crack spacing vs. strain and (b) comparison of tensile stress vs. strain from strain gage measurements and cross-head displacement.

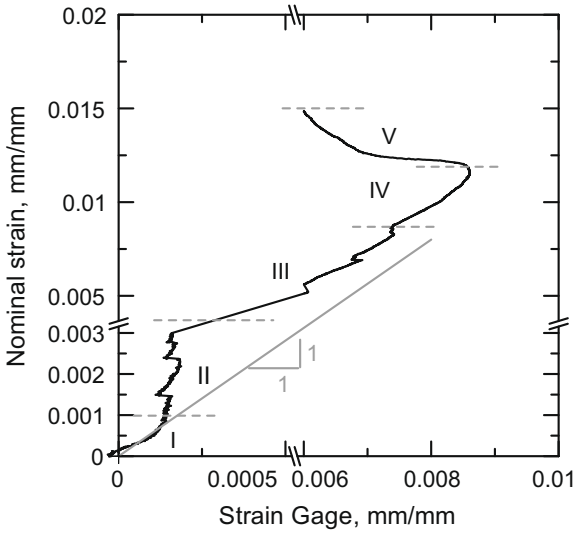

Fig. 6. Relationship between the strain gage and strain measured by the stroke.

From a macroscopic perspective, the bend over point (BOP) corresponds to the formation of matrix cracking. Five distinct zones are identified using roman numerals with two zones prior to and three zones after the bend over point (BOP). Fig. 5b shows both the initial response and also the overall response of the stress strain curve using a multi-scale axis representation. Fig. 6 shows the relationship between the strain gage reading and the strain measured by the stroke. Note that the measurements of these two gages allow differentiation of the response ranges. Zone I corresponds to the elastic-linear range where both matrix and the fiber behave linearly. Due to low volume fraction of fibers ($\leqslant$10%) the stiffness of the composite is dominated by matrix properties and this zone is limited to strain measures of up to 150–175 μstr as shown by the inset of Fig. 6. The initial stress–strain response is marked by a limited range of linear-elastic portion as the two strain measures are almost the same, and the specimen exhibits the highest stiffness. The deviation from linearity occur at around 150 microstrains due to initiation and propagation of first cracks. Note that the sensitivity of the stroke displacement in this range is within the instrumentation error, therefore, the strain gage response is far more reliable than the stroke in this range. The linear zone is terminated by initial crack formation in the matrix phase (reported as of σ_{BOP-} from experiments) as shown in Fig. 5a. After

Table 1
Crack spacing vs. strain parameters for tension and bending tests. Parameters were computed for four different specimens. Identification of specimens (i.e. specimen #) corresponds to the same as of Table 2 (SD = standard deviation).

Tests	Specimen #	$S_1 + S_0 e^{-\alpha(\varepsilon_i - \varepsilon_{mu})}$			
		S_1	S_0	α	ε_{mu} (mm/mm) – tension δ_{mu} (mm) – bending
Direct tension	2	24.8	318.63	666.66	0.0015
	4	25.64	324.93	680.27	0.0016
	5	13.79	135.8	288.18	0.0013
	6	24.23	539.18	1204.81	0.0015
	Mean ± SD	22.1 ± 5.5	329.6 ± 164.9	709.7 ± 376.2	0.00155 ± 0.000153
Bending	1	38.05	126.82	0.25	0.99
	2	41.58	171.95	0.24	0.99
	3	54.57	289.83	0.41	1.49
	5	23.74	346.47	0.26	4.5
	Mean ± SD	39.5 ± 11.1	233.8 ± 101.8	0.26 ± 0.07	1.99 ± 1.68

the initiation of cracks in the matrix, its load carrying capacity does not vanish as the cracks are bridged by the longitudinal fibers.

Immediately after the initiation of the first matrix crack, other matrix cracks also initiate throughout the specimen at approximately regular intervals and begin to propagate across the width [20]. The strain recorded by the resistance gage remains relatively constant in this range which indicates a steady state condition of several cracks that initiate and propagate across the width of the specimen. The strain range within Zone II is associated with formation of matrix cracks, however, no single crack has traversed the entire width. The term defined as BOP^+ corresponds to the stress level at which the first matrix crack completely propagates across the width. As indicated in the experimental results shown in Fig. 5a and b the linear behavior terminates at the σ_{BOP-} = 3.63–4.80 MPa. The bend over point ranges from the beginning of non-linearity at 4.80 MPa to a point where the slope drastically decreases ($\sigma_{BOP}+$ = 4.80–5.59 MPa). Zone II is therefore defined as the stable cracking range between the two stress levels of σ_{BOP-} and $\sigma_{BOP}+$.

The post BOP stage is characterized by formation of distributed cracking in Zone III. In this homogenization phase, as the applied strain increases, more cracks form and the spacing decreases in an exponential manner as presented empirically by Eq. (1). The strain measured by the strain gage remains constant while several cracks form throughout the section as shown in Fig. 5b. The decrease in crack spacing can be empirically represented as a function of three parameters and its initiation is represented by parameters S_0, S_1, α, and $_{mu}$ (Eq. (1))

$$S(\varepsilon_i) = S_1 + S_0 e^{-\alpha(\varepsilon_i - \varepsilon_{mu})} \quad \varepsilon_i > \varepsilon_{mu} \tag{1}$$

where $S(\varepsilon_i)$ = crack spacing as a function of strain, ε_{mu} = average strain at the BOP level, or where the first set of measurements were obtained, ε_i = independent parameter representing strain in the specimen, S_0 and α = constants representing the initial length of the specimen and rate of crack formation as a function of strain, and S_1 = saturation crack spacing. The stiffness of the sisal fiber reinforced cement composite system is sufficiently high and keeps the newly formed cracks from widening; thus promoting multiple cracking behavior as shown in Fig. 5. This stiffness affects the rate of reduction of crack spacing, or α parameter. Individual, mean and standard deviations values of the S_1, S_0, ε_{mu} and α for the composites studied under tension and bending loads are presented in Table 1. The mentioned parameters were computed from four different specimens. Significant variations in the value of the α parameter were observed in the tensile tests. Less variability was obtained for S_1, S_0, and α from the bending tests.

The crack spacing measurements as shown in Fig. 5a show a general reduction in spacing during loading until a steady state condition is reached. This zone covers a large range at the end of Zone II, and III and remains constant throughout Zone IV. This constant level of crack spacing is defined as saturation crack spacing. Beyond this point, reduction in crack spacing is not observed since no new cracks form, while, as verified by the pictures of the specimen under the load, additional imposed strain results in widening of the existing cracks.

It can be seen from Fig. 5a that at the strain of 0.0016 mm/mm (Zone III) the cracking spacing drastically decreases from an initial value of 130 mm to 45 mm. During the multiple crack formation the crack spacing decreases until a point (beginning of Zone IV) where it becomes constant at 23 mm.

Zone IV corresponds to the completion of cracking phase and initiation of debonding. Note that the strain gage recording fails to increase as the same rate of the overall strain measure and no additional cracks are formed. As the cracking saturates in the specimen, Zone IV is dominated by progressive damage and characterized by a crack widening stage ultimately leading to failure by fiber

Table 2
Summary of tensile and four-point bending results (CHD = cross-head displacement, SG = strain gage and SD = standard deviation).

Tests	Instrumentation	Specimen #	$E_{initial}$ (GPa)	$\sigma_{BOP(-)}\sigma_{LOP(-)}$ (MPa)	$\sigma_{BOP(+)}\sigma_{LOP(+)}$ (MPa)	$\varepsilon_{BOP(-)}\ \varepsilon_{LOP(-)}$ (%)	$\varepsilon_{BOP(+)}\ \varepsilon_{LOP(+)}$ (%)	E_{pc} (GPa)	$\sigma_{ultimate}$ (MPa)	$\varepsilon_{ultimate}$ (%)	Total toughness (kJ/m^2)	First crack toughness (kJ/m^2)
Direct tension	CHD	1	9.23	3.63	4.8	0.023	0.043	0.40	12.40	2.2	49.14	1.66
		2	8.26	4.25	4.87	0.074	0.098	0.49	10.61	1.35	40.74	1.82
		3	12.58	4.50	5.08	0.021	0.049	0.59	14.70	1.73	66.00	1.77
		4	8.38	4.34	4.85	0.038	0.067	0.43	11.32	1.27	39.35	1.74
		5	9.44	4.86	5.59	0.053	0.076	0.56	12.74	1.53	46.22	1.79
		6	9.05	4.60	5.15	0.071	0.085	0.52	10.56	1.15	34.20	1.41
		Mean ± (SD)	9.49 (1.58)	4.36 (0.41)	5.10 (0.30)	0.046 (0.023)	0.069 (0.021)	0.50 (0.07)	12.00 (1.57)	1.53 (0.38)	45.95 (11.15)	1.70 (0.15)
	SG	6	34.17	–	–	0.015	0.017	1.32	–	0.80	–	–
Bending	CHD	1	–	10.1	10.2	–	–	–	28.47	–	15.45	0.25
		2	–	9.58	9.64	–	–	–	29.31	–	26.84	0.11
		3	–	7.78	8.94	–	–	–	29.85	–	34.43	0.28
		4	–	8.58	10.08	–	–	–	20.88	–	17.51	0.71
		5	–	9.24	10.07	–	–	–	23.67	–	19.85	0.92
		6	–	8.06	8.65	–	–	–	18.26	–	18.68	0.62
		Mean ± (SD)	–	8.89 (0.90)	9.60 (0.51)	–	–	–	25.07 (4.86)	–	22.13 (7.16)	0.48 (0.31)
	SG	2	35.32	–	–	–	–	–	–	–	–	–
		3	28.72	–	–	–	–	–	–	–	–	–
		4	16.15	–	–	0.04	0.07	*0.50	–	0.60	–	–
		5	24.61	–	–	0.02	0.03	*0.51	–	1.00	–	–
		6	18.07	–	–	–	–	–	–	–	–	–
		Mean ± (SD)	29.55 (8.02)	–	–	0.03 (0.014)	0.05 (0.028)	0.50 (0.006)	–	0.80 (0.28)	–	–

* Computed at Zone II (refer to Fig. 8a).

pullout. This zone is asymptotically terminated at the saturation crack spacing represented by parameter S_1. The dominant mechanism of failure during stage IV is crack widening which is associated with fiber debonding and pullout. The post peak response occurs in Zone V where a residual strength of approximately 2 MPa is observed. As shown in Table 2 a considerable difference between the initial ($E_{initial}$) and post-crack (E_{pc}) moduli from cross-head displacement data and strain-gages are observed. Results for $E_{initial}$ and E_{pc} from strain-gages are, respectively, 3.6 and 2.60 times greater than that of the cross-head. This discrepancy is attributed to the spurious deformation, slipping, and localized damage at the grips, indicating that initial stiffness computation from the cross-head displacement is significantly erroneous.

The average ultimate tensile strain of the composite is 1.53% (measured from cross-head displacement) which shows the capacity of the sisal fibers to cause crack distribution. Strain values ranging from 1.15% to 2.2% was obtained for individual tests. The average ultimate tensile strength of 12 MPa and an initial modulus of 34.17 GPa (computed from strain gage measurements) is indicative that sisal fiber reinforced cement composite presents a mechanical performance high enough for structural level applications. Nevertheless, a small variability was observed when addressing individual tensile tests. Ultimate strength ranged from 10.56 to 14.70 MPa as can be seen in Table 2.

Fig. 7a shows the typical bending response of the sisal fiber reinforced composite and its crack spacing measurements. Using the same methodology as for the direct tension, the bending curve

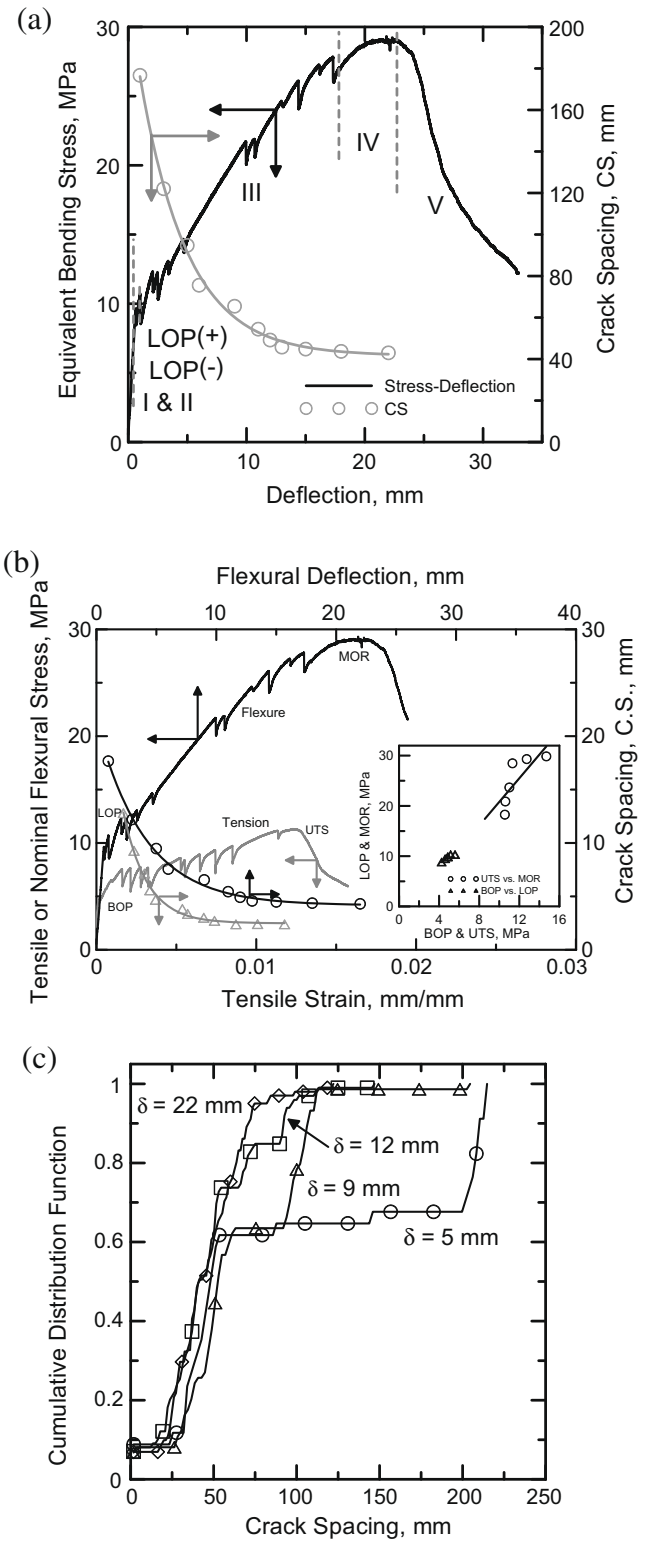

Fig. 7. Bending response of the sisal fiber reinforced composite system: (a) bending stress and crack spacing vs. displacement, (b) comparison of flexural vs. tensile response and (c) cumulative distribution function for crack spacing.

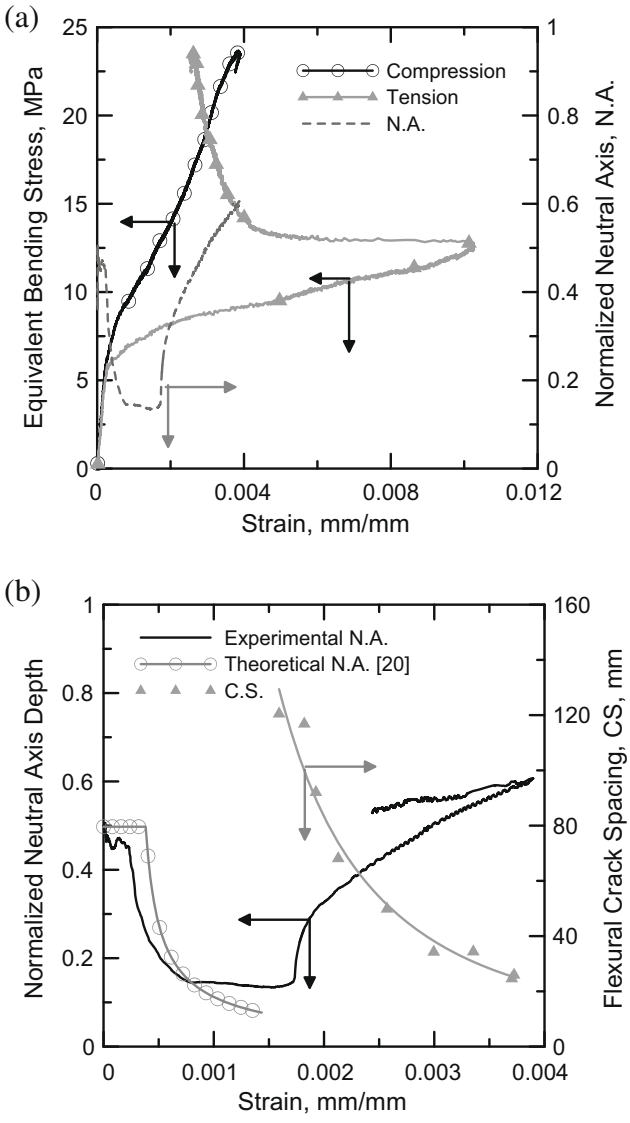

Fig. 8. Neutral axis computation: (a) compression and tension strains under four-point bending loading and (b) crack spacing vs. neutral axis.

was divided into 5 regions identified by roman numerals. Zone I corresponds to the elastic-linear range where both matrix and the fiber behave linearly. The lower and upper bounds of the limit of proportionality (LOP) delimit the Zone II. Mean values of 8.89 and 9.60 MPa for σ_{LOP}^{-} and σ_{LOP}^{+}, respectively, were obtained. The post LOP range (Zone III) is characterized by a multiple cracking formation which can be represented by an exponential decay function similar to Eq. (1) (see Table 1). Fig. 7a shows that the crack spacing initially drops abruptly from 180 mm to 60 mm up to the deflection of 10 mm. The crack spacing saturates at the end of Zone IV (40 mm) which happens at a deflection of approximately 23 mm. Zone V is characterized by the strain softening response due to the localization and widening of a major crack. No new cracks appear at this stage and crack spacing remains constant. The initial elastic modulus of 29.55 GPa shows that the replacement of cement by calcined clays resulted in a matrix of sufficiently high stiffness.

The bending and tensile responses with their respective crack distribution are compared in Fig. 7b. The inset plot shows the relationship between LOP vs. BOP and MOR (modulus of rupture) vs. UTS (ultimate tensile stress). It can be seen that under bending, loads associated with the formation of the first crack occur at stress levels twice as those observed for the direct tension tests. The correlation of tensile and bending test results has been documented through theoretical modeling [21]. It has been shown that the flexural results are affected by tension stiffening effects and normalization of the flexural load with an elastic section modulus may result in apparent tensile strength which are as high as 2.8 times the tensile strength. At these stress levels a homogeneous response was observed for all composites. A greater variability was noticed under both testing conditions at ultimate stress states. The values reported for MOR is approximately two times greater than that of the UTS. A procedure to theoretically validate this ratio has been shown for a variety of strain hardening cement composite systems [21]. Under flexural loads, the saturation crack spacing is twice as large as that of tensile loads.

Fig. 7c shows the cumulative distribution function for crack spacing under bending at four different levels of displacement beyond the LOP range. As the displacement level increases from 5 to 12 mm, the variability in measured crack widths decreases. As the displacement level approaches the crack saturation level, a more homogenized set of data with less scatter is observed. At this level 99% of the measurements are below 75 mm.

The composite toughness was determined as the area under the load–displacement curve for tension and bending tests. Elevated toughness values of 45.95 and 22.13 kJ/m^2 in tension and bending, respectively, demonstrated the high ductility capacity of the sisal fiber composite. Toughness at first crack strength was computed for tensile and bending tests as 1.70 and 0.48 kJ/m^2, respectively. These values represent a ratio of total to first crack toughness of 27 and 46.1, respectively.

The compressive and tension strains during a four-point bending test are shown in Fig. 8a. A distinct behavior is observed after the first crack formation. Three different zones are identified for the compressive strain. Zone I is the linear-elastic region which yields the same stiffness (29.55 GPa) as the tension strain. Zone II begins after the first crack formation and is characterized by an increase in stiffness during the multiple cracking. Although not shown, the unloading process is defined by Zone III. At this range a modulus of 8.0 GPa is reported.

The tensile region of the flexural sample experiences five ranges of behavior. Zone I is characterized by a linear-elastic response. After the complete formation of the first crack, Zone II begins. Stiffness degradation is caused by the crack formation, and results in a significant drop in the modulus from 29.55 to 0.50 GPa. A decrease in tensile strain occurs in zone III and IV as a result of crack formations in the vicinity of the strain gage and shear lag mechanisms which result in stress decay in matrix. Note that the resistance type strain gage measurements are not uniquely related to the uncracked material as the strain recorded in the matrix is dependent on the relative position of a strain gage between two parallel cracks. At Zone IV the strain gage response of the matrix between two cracks results in a stiffness of 10.7 GPa. This stage characterizes the degraded matrix's contribution to the composite overall response. Finally, Zone V is the unloading region that presents a stiffness of 22.94 GPa which is similar to Zone I. The data acquisition of strains from the compression and tension faces during the bending test allowed the computation of the neutral axis (normalized with specimen depth, d) as seen in Fig. 8a and b. During the elastic-region zone the normalized neutral axis depth (NA)

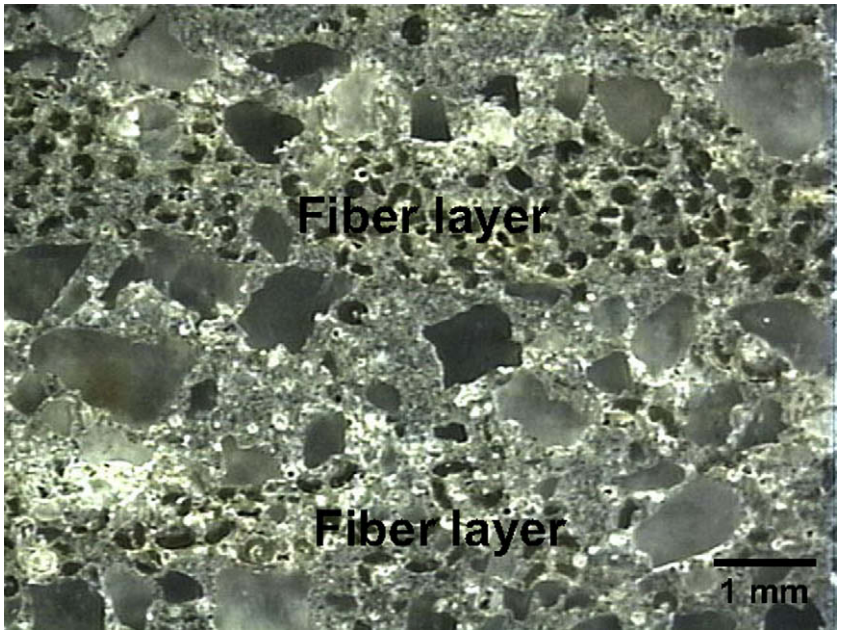

Fig. 9. Optical micrograph showing the cross-section view of a sisal fiber reinforced composite before testing.

remains constant at centroidal location (0.5d) until the beginning of the first crack formation which happens at 0.00023 mm/mm. A sudden drop of the NA to 0.18d is observed as tensile cracking results in load redistribution across the thickness. This NA value indicates that assuming plane sections remaining plane, 82% of the sample is in tension while the rest is in compression for strains up to 0.002 mm/mm. At this strain level the first crack has already been formed and the crack spacing starts to decrease with an increase in the NA until a strain level of 0.004 mm/mm (see Fig. 8b).

Analysis of tensile and compressive stress and strain distribution are important since they provide an insight into the role that cracking plays in redistributing the forces applied onto the member. Flexural loads are carried by means of tensile cracking and redistribution of stresses. Simplifying assumptions which are based on uncracked section modulus leading to an equivalent elastic stresses are unconservative and significantly overestimate the strength of the material.

4.2. Microstructure

Fig. 9 shows an optical micrograph cross-section view of the sisal fiber reinforced composite with two layers of sisal fibers embedded in the matrix. The matrix has sufficiently penetrated within and is surrounding all the fibers, indicating that the matrix rheology was adequate for the manufacturing of the composite system.

A SEM micrograph showing the sisal fiber composite at the end of the tensile test is presented in Fig. 10. The contribution of the sisal fibers to crack arrest and bridging mechanism is observed. The crack propagates through the thickness of the specimen from one fiber layer to the next (Fig. 10a and b). Crack deflection mechanism occurs due to interface delamination and changes in the crack path. Such crack arresting and bridging mechanisms lead to a ductile composite as shown by the tensile and bending responses (Figs. 5 and 7).

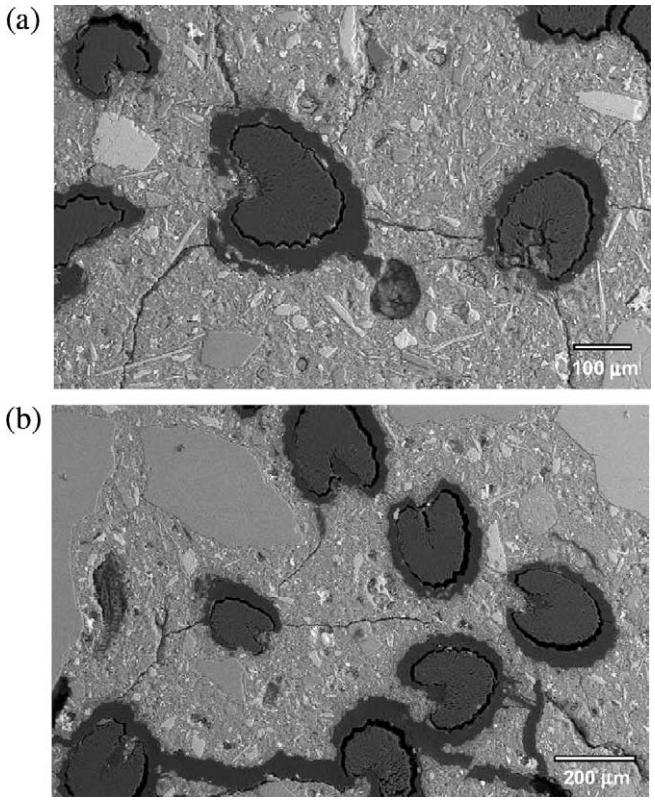

Fig. 10. SEM micrographs showing crack arresting and bridging in a sisal fiber reinforced composite after a tensile test.

5. Conclusion

A study on the cracking formation under tensile and bending load of continuous sisal fiber cement composites was presented and mechanisms of crack formation and toughening were addressed. Use of continuous sisal fabrics that are formed by aligning and stitching the fibers in a multilayer cement composite system present a new perspective for the use of natural fiber reinforced composites in the construction industry. A matrix with a low content of Portland cement and Calcium Hydroxide was used to reduce the potential aging of sisal fibers.

The composites showed high modulus at linear-elastic zones ranges with elastic moduli in the range of: 30–34 GPa under flexural and direct tension, respectively.

Multiple cracking behavior was observed under both tensile and bending loads. The crack spacing as a function of applied strain was characterized using an exponential decay function under both loading conditions. The crack saturation spacing in tension was almost half of its corresponding values in flexure. While the post-crack modulus decreased significantly compared to the elastic response, the composite was able to reach average ultimate strengths of 12 and 25 MPa under tension and bending loads, respectively.

The high energy absorption capacity of the developed composite system was reflected in high toughness values under tension and bending loads of approximately 45 and 22 kJ/m^2, respectively.

Microstructural analysis indicated that the sisal fibers were able to bridge and arrest the cracks within the tensile region of response leading to a high mechanical performance and energy absorption capacity.

Acknowledgement

The authors acknowledge the Brazilian Agency CNPq for its partial financial support.

References

[1] Swift DF, Smith RBL. The flexural strength of cement-based composites using low modulus (sisal) fibers. Composites 1979;6(3):145–8.
[2] Coutts RSP, Warden PG. Sisal pulp reinforced cement mortar. Cement Concrete Comp 1992;14(1):17–21.
[3] Toledo Filho RD, Ghavami K, England GL, Scrivener K. Development of vegetable fiber-mortar composites of improved durability. Cement Concrete Comp 2003;25(2):185–96.
[4] Toledo Filho RD, Scrivener K, England GL, Ghavami K. Durability of alkali-sensitive sisal and coconut fibers in cement mortar composites. Cement Concrete Comp 2000;22(2):127–43.
[5] Toledo Filho RD, Joseph K, Ghavami K, England GL. The use of sisal fiber as reinforcement in cement based composites. Braz J Agr Environ Eng 1999;3(2):245–56.
[6] Silva FA, Ghavami K, d'Almeida JRM. Toughness of cementitious composites reinforced by randomly sisal pulps. In: 11th international conference on composites engineering. Hilton Head Island; 2004.
[7] Silva FA, Ghavami K, d'Almeida JRM. Bamboo-wollastonite hybrid cementitious composites: toughness evaluation. In: Joint ASME/ASCE/SES conference on mechanics and materials, Baton Rouge; 2005.
[8] Silva FA, Ghavami K, d'Almeida JRM. Behavior of CRBP-AL composites subjected to impact load. In: 17th ASCE engineering mechanics conference, Delaware; 2004.
[9] Mobasher B, Pivacek A, Haupt GJ. Cement based cross-ply laminates. J Adv Cement Based Mater 1997;6:144–52.
[10] Silva FA, Melo Filho JA, Toledo Filho RD, Fairbairn EMR. Effect of reinforcement ratio on the mechanical response of compression molded sisal fiber textile reinforced concrete. In: High performance fiber reinforced cement composites (HPFRCC5), Mainz; 2007. p. 175–82.
[11] Hagger J, Will N, Aldea C, Brameshuber W, Brockmann T, Curbach M, Jesse J. Applications of textile reinforced concrete. In: Brameshuber W, editor. State-of-the-art report of Rilem Technical Committee 201-TRC: textile reinforced concrete; 2006. p. 237–66.

[12] Silva FA, Melo Filho JA, Toledo Filho RD, Fairbairn EMR. Mechanical behavior and durability of compression moulded sisal fiber cement mortar laminates (SFCML). In: First international RILEM conference on textile reinforced concrete (ICTRC), Aachen, proceedings; 2006. p. 171–80.
[13] Toledo Filho RD, Silva FA, Fairbairn EMR, Melo Filho JA. Durability of compression molded sisal fiber reinforced mortar laminates. Construct Build Mater 2009;23:2409–20.
[14] Silva FA, Chawla N, Toledo Filho RD. Tensile behavior of high performance natural (sisal) fibers. Comp Sci Technol 2008;68:3438–43.
[15] Mukherjee KG, Satyanarayana KG. Structure and properties of some vegetable fibres. Part 1: sisal fibre. J Mater Sci 1984;19:3925–34.
[16] Brazilian Standard NBR 11578. Cimento Portland Composto. Associação Brasileira de Normas Técnicas (ABNT); 1991 [in Portuguese].
[17] Mobasher B, Peled A, Pahilajani J. Distributed cracking and stiffness degradation in fabric cement composites. Mater Struct 2006;39:317–31.
[18] Mobasher B, Stang H, Shah SP. Microcracking in fiber reinforced concrete. Cement Concrete Res 1990;20(5):665–76.
[19] Stang H, Mobasher B, Shah SP. Quantitative damage characterization in polypropylene fiber reinforced concrete. Cement Concrete Res 1990;20(4): 540–58.
[20] Mobasher B, Castro-Montero A, Shah SP. A study of fracture in fiber reinforced cement-based composites using laser holographic interferometry. Exp Mech 1990;30:286–94.
[21] Soranakom C, Mobasher B. Correlation of tensile and flexural responses of strain softening and strain hardening cement composites. Cement Concrete Comp 2008;30:465–77.